

Biocompatibility and biofouling of MEMS drug delivery devices

Gabriela Voskerician^{a,b}, Matthew S. Shive^a, Rebecca S. Shawgo^c, Horst von Recum^d,
James M. Anderson^{a,b,e,*}, Michael J. Cima^c, Robert Langer^e

^a Department of Biomedical Engineering, Institute of Pathology, Case Western Reserve University, 2085 Adelbert Road,
10900 Euclid Avenue, Cleveland, OH 44106, USA

^b Institute of Pathology, Case Western Reserve University, 2085 Adelbert Road, Cleveland, OH 44106, USA

^c Department of Material Science and Engineering, Massachusetts Institute of Technology, 77 Massachusetts Avenue, Cambridge, MA 02139, USA

^d Department of Chemical Engineering, Massachusetts Institute of Technology, 77 Massachusetts Avenue, Cambridge, MA 02139, USA

^e Department of Macromolecular Sciences, Case Western Reserve University, 10900 Euclid Avenue, Cleveland, OH 44106, USA

Received 16 May 2002; accepted 26 November 2002

Abstract

The biocompatibility and biofouling of the microfabrication materials for a MEMS drug delivery device have been evaluated. The *in vivo* inflammatory and wound healing response of MEMS drug delivery component materials, metallic gold, silicon nitride, silicon dioxide, silicon, and SU-8TM photoresist, were evaluated using the cage implant system. Materials, placed into stainless-steel cages, were implanted subcutaneously in a rodent model. Exudates within the cage were sampled at 4, 7, 14, and 21 days, representative of the stages of the inflammatory response, and leukocyte concentrations (leukocytes/ μ l) were measured. Overall, the inflammatory responses elicited by these materials were not significantly different than those for the empty cage controls over the duration of the study. The material surface cell density (macrophages or foreign body giant cells, FBGCs), an indicator of *in vivo* biofouling, was determined by scanning electron microscopy of materials explanted at 4, 7, 14, and 21 days. The adherent cellular density of gold, silicon nitride, silicon dioxide, and SU-8TM were comparable and statistically less ($p < 0.05$) than silicon. These analyses identified the MEMS component materials, gold, silicon nitride, silicon dioxide, SU-8TM, and silicon as biocompatible, with gold, silicon nitride, silicon dioxide, and SU-8TM showing reduced biofouling.

© 2003 Elsevier Science Ltd. All rights reserved.

Keywords: Biocompatibility; Biofouling; MEMS component materials; Exudate analysis; Material surface analysis

1. Introduction

A wide variety of devices are being developed that take advantage of the materials and processing tools of microfabrication for applications in medicine and biology [1–4]. As a result of the advances made by the microelectronics industry, the advantage of such devices consist of their microsize potentials and the ability to be manufactured in high volume with low unit cost. However, devices such as biological microelectromechanical systems (BioMEMS), ion sensing field effect transistors (ISFET) or silicon-based microelectrodes

had performed well *in vitro*, but experienced significant biofouling *in vivo*, over time [5–7].

Silicon-based MEMS technology is starting to impact the drug delivery field with the development of micro-needles [8] and immunisolating biocapsules [9]. Quantitative biocompatibility and biofouling data are needed to aid not only in device material selection for medical applications, but also to further understand the *in vivo* interactions between the emerging technology and the biological environment.

We have developed a silicon-based implantable drug delivery system that uses elemental gold membranes to seal individual drug-filled reservoirs (Fig. 1) [10]. This device allows individual packaging and sealing of compounds, coupled with the ability to individually access the membranes sealing the reservoirs through a targeted electrochemical reaction (anode/cathode). The goal of the MEMS delivery device is to release specific

*Corresponding author. Department of Biomedical Engineering, Institute of Pathology, Case Western Reserve University, 2085 Adelbert Road, 10900 Euclid Avenue, Cleveland, OH 44106, USA. Tel.: +1-216-844-1002; fax: +1-216-844-8004.

E-mail address: gxv4@po.cwru.edu (J.M.A. Anderson).

therapeutic agents in complex dosing patterns. The device can be used for the release of hormones, chemotherapeutic agents, analgesics, anesthetics, and other bioactive agents.

Any device intended for long-term *in vivo* applications has to fulfill rigorous biocompatibility and biostability requirements [11]. First, it should not induce toxicity in the surrounding tissues, and should not damage the local tissue due to induced mechanical stresses. Second, the drug-eluting capabilities of the MEMS device should not be compromised by the surrounding tissue. Specifically, the implant must tolerate long-term exposure to the physiological environment, as well as resist the impact of the surrounding tissue on its function (biofouling) [12].

With this in mind, we have investigated the leukocyte behavior and cellular adhesion in a rat model as indicators of biocompatibility and biofouling for materials used in the manufacturing of MEMS delivery

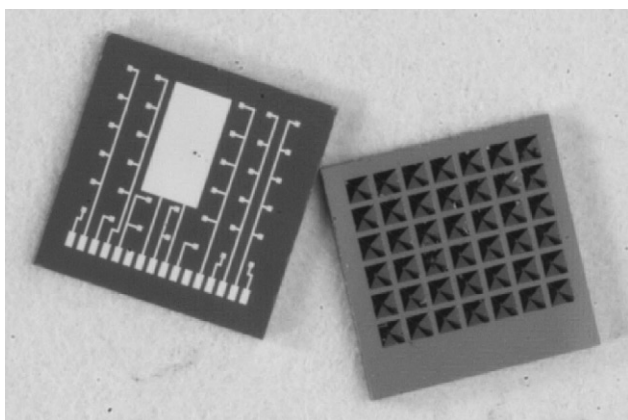


Fig. 1. Drug delivery microchip device: top view of electrode and reservoir modules.

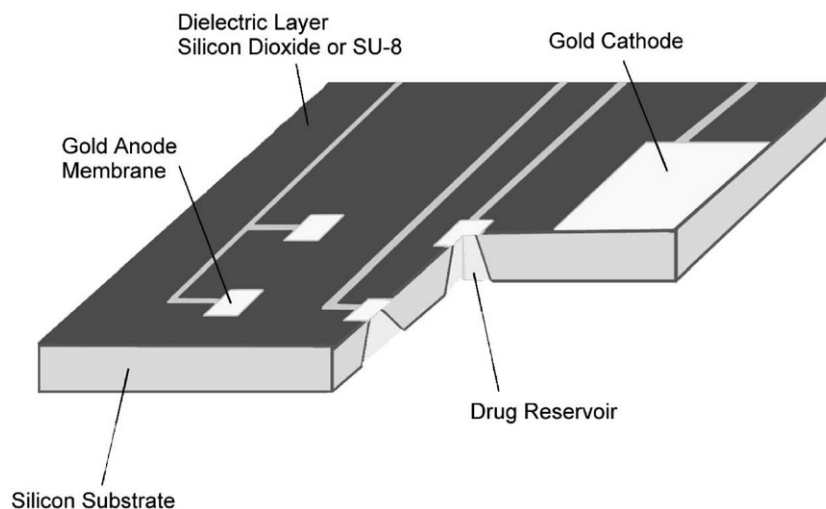


Fig. 2. Schematic of an MEMS drug delivery device showing the component materials.

systems, specifically, metallic gold, silicon, silicon dioxide, silicon nitride, and SU-8TM photoresist (Fig. 2). The MEMS device used the gold film to manufacture the electrodes, silicon as a substrate and structural material, silicon dioxide and silicon nitride were used for their dielectric and structural properties, and SU-8TM was used for its near-UV photoresist as well as dielectric properties. SU-8TM composition is based on a multifunctional bisphenol A novolak epoxy resin and a photoacid generator as the curing agent, as disclosed by IBM [13]. Understanding the material–tissue interaction that results from *in vivo* implantation is an important step in the development of viable, long-term implantable MEMS delivery devices.

2. Materials and methods

2.1. Fabrication of MEMS drug-delivery device

Material samples of macroscopic size were obtained using processes in the fabrication of drug delivery MEMS [10,14]. Polished silicon wafers (Wafernet Inc., San Jose, CA) were used as the substrate for the other materials. Wafers were coated with 3000 Å of silicon nitride (VTR—SVG/Thermco 7000 Series vertical tube reactor) using a 10:1 ratio of the gas flows of dichlorosilane and ammonia. Other wafers were coated with 100 Å of a chromium adhesion layer and 3000 Å of gold in an electron beam evaporator (Temescal Semiconductor Products Model VES 2550). Each wafer was cut into sections 9 mm × 15 mm.

The fabrication of drug delivery MEMS devices has been previously described and is schematically illustrated in Fig. 3. Silicon nitride was deposited onto 300 μm thick silicon wafers (Wafernet Inc., San Jose, CA). Positive photoresist (Arch Chemicals OCG825-20)

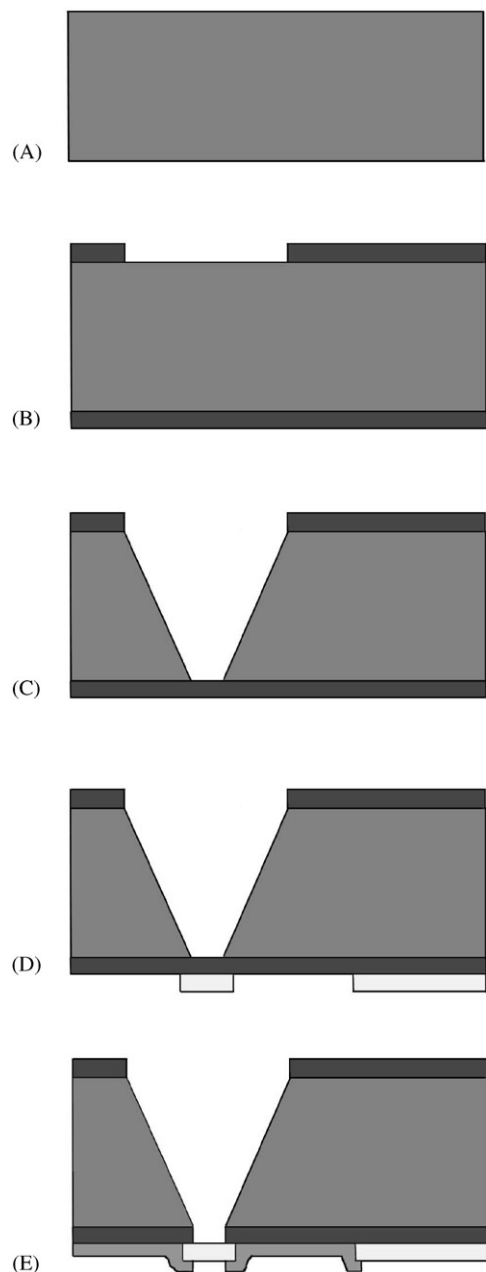


Fig. 3. Device Fabrication: (A) A silicon substrate is (B) coated with silicon nitride and patterned into reservoir openings. (C) Reservoirs are etched in KOH solution. (D) Gold is deposited and patterned into electrodes, and (E) the dielectric layer is deposited and patterned to expose the anodes and cathode.

was used to define the large openings of the reservoirs, and the silicon nitride was removed from those openings using reactive ion etch (Plasmaquest Series II Reactor Model 145). The nitride acted as a mask and etch stop when the square pyramidal reservoirs were etched in KOH solution. Next, the gold electrode pattern was defined using negative photoresist (Crariant AZ5214 E). The chromium and gold were evaporated onto the wafers and then the pattern defined by removal of the

resist. Two types of dielectric were used for different wafers. Plasma enhanced chemical vapor deposition (Astex Series III, Wilmington, MA) was used to deposit silicon dioxide. The oxide was patterned with the positive photoresist and reactive ion etched, while SU-8TM (SU-8 5, MicroChem Corp, Newton MA) was directly patterned.

2.2. Cage fabrication

Test specimens of all component materials, gold, silicon, silicon dioxide, silicon nitride, and SU-8 dielectric were placed singly into cylindrical stainless steel wire mesh cages measuring approximately 3.5 cm long and 1.0 cm in diameter. The mesh from which the cages were made was type 310 stainless steel with a mesh size of 24, a wire diameter of 0.254 mm (0.01 in), and interstices measuring $0.8 \times 0.8 \text{ mm}^2$ (Cleveland Wire Cloth and Manufacturing Co, Cleveland, OH). Prior to cage fabrication, the mesh was sonicated in ethanol (Pharmaco Products Inc., Brookfield, CT) for 15 min, followed by a 10 min rinse with distilled water. Cages containing the respective materials were ethylene oxide sterilized (Amsco model 2057 sterilizer, University Hospitals of Cleveland, OH) using an exposure time of 1 h and 45 minutes at 130°F and an outgassing time of 12 h at 120°F .

2.3. Implantation

Sterilized cages were implanted subcutaneously and bilaterally in the posterior areas of the back of female Sprague–Dawley rats 12 weeks old (Charles Rivers Laboratories, North Wilmington, MA) two cages per animal observing IACUC and NIH animal-care guidelines. Aerrane (Baxter, Deerfield, IL) was used in a continuous analgesic stream to keep the animals unconscious during implantation. The rats were shaved and their skin scrubbed with surgical grade Betadine (The Purdue Frederick Co., Stamford, CT). An incision 1.0–1.5 cm long was made in the skin about 2 cm above the tail and along the midline. Then, 0.5% Marcaine solution (Abbott Laboratories, North Chicago, IL), a local anesthetic, was applied onto the incision to minimize post-operative discomfort. Blunt dissection was used to prepare an implant pocket in the facial plane beneath the panniculus carnosus muscle from the underlying tissue from the incision to just above the hip. The sterile cage containing the material was then introduced through the incision and positioned within the pocket and away from the incision site. The incision was then closed with 9 mm stainless steel surgical wound clips (Becton Dickinson, Sparks, MD) and washed with Betadine. Sterile surgical techniques were observed. In addition, empty cages were gas sterilized and implanted into a separate group of animals as controls. The rats

were maintained on Purina Rat Chow and water ad libitum at the Animal Research Facilities of Case Western Reserve University on 12 h light/dark cycles.

2.4. Exudate analysis

At 4, 7, 14, and 21 days post-implantation the inflammatory exudate, which collects within the cage in response to the presence of the cage and the test material, was aspirated using a 27 1/2-gauge needle and a 1 cc tuberculing syringe (Becton Dickinson, Franklin Lakes, NJ) and placed in a microsample tube (Fisher Scientific, Pittsburgh, PA). Not more than 0.5 cc of exudate was removed at once, and exudates were not withdrawn from the same animal twice in any 7 day period. Immediately after withdrawal, an aliquot of each exudate was cultured on brain–heart infusion agar plates (Department of Microbiology, Case Western Reserve University, Cleveland, OH), incubated for 48 h at 37°C to check for bacterial infection. Infected exudates as well as those with an appreciable amount of erythrocyte contamination were removed from further analysis.

Exudate white blood cell concentrations, cells per μl , were determined on each sample mixture using a hemacytometer (Baxter, McGaw Park, IL). Following cell re-suspension within the exudates, 10 μl sample of each exudate was mixed with 40 μl of dilute Wright's stain solution (Sigma Diagnostics, St. Louis, MO). Both sides of the hemacytometer were loaded with the cell suspension covering the counting grids. Cells were counted in the four edge squares and the center square (total of 10 squares) using the 20 \times microscope lens. The total number of cells counted was divided by ten to obtain the average number of cells per square. Using the manufacturer's information that each square holds a 1 μl volume, the following formula was suggested by the manufacturer in determining any cell concentration, in the present case, the leukocyte concentration (Total Leukocyte Concentration, TLC) of each exudate sample:

$$\begin{aligned} \text{TLC} &= \text{average number of cells/square} \times \text{square}/\mu\text{l} \\ &= \text{average number of cells}/\mu\text{l}. \end{aligned}$$

Based on these cell counts, a volume of exudate containing 70,000 cells was mixed with RPMI Medium (Gibco Laboratories, Grand Island, NY) to make 700 μl of cell suspension. Aliquots (200 μl) of this suspension were spun down onto pre-cleaned glass microslides using a Shandon Cytospin 2 Centrifuge (Shandon Southern Instruments Inc., Sewickley, PA), generating slides of approximately 20,000 cells for each exudate. The slides were stained with Wright's stain for differential leukocyte counts. A total of 200 cells per slide were counted at 40 \times under a light microscope and

differentiated as polymorphonuclear leukocytes (PMNs), monocytes/macrophages or lymphocytes.

2.5. SEM analysis

In addition to the exudate analysis, cages were explanted and the specimens retrieved at days 4, 7, 14, and 21 for SEM evaluation of adherent cells (biofouling). Upon retrieval, specimens were rinsed in sterile isotonic phosphate buffered saline (PBS) solution (Gibco, Grand Island, NY). The materials were then placed in a fixative solution containing 0.1 M cacodylate buffer, 4% sucrose, and 2.5% glutaraldehyde (Sigma, St. Louis, MO), stored at 4°C. Following fixation, materials were rinsed thoroughly in distilled water then gradually dehydrated using a series of ethanol solutions of increased concentrations (30%–50%–70%–95%–100% ethanol). The materials were treated twice (30 min/treatment) with hexamethyl-disilizane (Sigma, St. Louis, MO), a drying agent. Following drying, they were sputter coated with gold–palladium (Polaron ES100 II Sputter Coater, Polaron Equipment Ltd., Watford, UK) and examined by scanning electron microscopy, (SEM) (JEOL Model JSM-840A, JEOL USA Inc., Peabody, MA). Using SEM, the cellular density present at all time point on each explanted material was determined (cells/ mm^2). In addition, adherent cellular morphologies of materials at each time point were investigated.

2.6. Statistical analysis

The data from all material groups were compared to that of the empty cage controls. Statistical analysis was carried out using the unpaired Student t-test on StatView™ software. A *p*-value of less than 0.05 was considered statistically significant.

3. Results

3.1. Exudate analysis

Analysis of the inflammatory exudate within the cage (Table 1) demonstrated that all materials, with the exception of silicon surfaces explanted at days 7 and 14, elicited similar acute and chronic inflammatory responses as the empty cage controls at all time points. Silicon at days 7 and 14 had a significantly higher ($p < 0.05$) leukocyte concentration (TLC). However, by day 21 the silicon TLC approached comparable empty cage control levels.

All materials induced the early acute inflammatory response characterized by high PMN levels comparable to the empty cage controls. The acute inflammatory responses resolved over the first 14 days of the study

Table 1
In vivo exudate leukocyte concentrations, cells/ μ l, of MEMS component materials

Surface	TIME (days)	Total leukocytes	PMN	Monocytes	Lymphocytes
Empty cage	4	117 \pm 17	23 \pm 5	89 \pm 14	6 \pm 1
	7	50 \pm 25	5 \pm 4	41 \pm 20	4 \pm 2
	14	25 \pm 0	1 \pm 0	16 \pm 6	9 \pm 6
	21	25 \pm 0	0	21 \pm 2	4 \pm 2
Silicon wafer	4	117 \pm 22	17 \pm 1	86 \pm 18	13 \pm 4
	7	92 \pm 17 ^a	13 \pm 4	68 \pm 9	12 \pm 5
	14	63 \pm 14 ^a	2 \pm 0	50 \pm 10	11 \pm 2
	21	43 \pm 8	0	29 \pm 6	11 \pm 6
Silicon nitride	4	117 \pm 33	9 \pm 1	93 \pm 14	14 \pm 2
	7	25 \pm 0	4 \pm 1	20 \pm 1	1 \pm 0
	14	25 \pm 0	0	16 \pm 2	9 \pm 2
	21	25 \pm 0	0	22 \pm 1	3 \pm 1
Gold	4	125 \pm 21	19 \pm 12	96 \pm 50	10 \pm 2
	7	33 \pm 9	6 \pm 2	26 \pm 5	2 \pm 1
	14	25 \pm 0	1 \pm 1	19 \pm 2	5 \pm 3
	21	25 \pm 0	0	20 \pm 2	5 \pm 2
Silicon oxide	4	125 \pm 3	28 \pm 7	87 \pm 2	10 \pm 3
	7	41 \pm 1	1 \pm 1	37 \pm 5	3 \pm 1
	14	25 \pm 2	0	21 \pm 2	4 \pm 1
	21	25 \pm 1	0	19 \pm 9	6 \pm 2
SU-8	4	127 \pm 5	28 \pm 2	88 \pm 7	11 \pm 4
	7	49 \pm 4	3 \pm 1	38 \pm 5	7 \pm 3
	14	25 \pm 0	0	21 \pm 5	4 \pm 3
	21	25 \pm 0	0	20 \pm 3	5 \pm 1

^aStatistically different when compared to the empty cage control ($p < 0.05$) at the same time period.

All values represent mean \pm standard error of mean of $n = 3$.

(Table 1) and the concentration of PMNs decreased to virtually zero by the third time point for all materials. At day 14, the predominant cell types were monocytes and lymphocytes. At day 21 the number of cells decreased to a minimal concentration for all materials and the empty cage controls. No overall trends indicative of an adverse reaction were noted over the 21 days exudate analysis period.

3.2. SEM analysis

SEM image analysis was used to quantify the populations of adherent macrophages and foreign body giant cells (FBGCs), as well as to investigate temporal changes in cellular morphology. The SEM method, as a material surface investigative tool, lacks reliability in determining the actual size of the FBGCs, which is traditionally reported as number of nuclei per FBGC. As a result, the actual size of the FBGCs was not reported. However, representative images of cell adhesion onto surfaces were acquired, and qualitative comparisons of size based on identical magnification

photomicrographs taken at different time points were inferred.

The number of macrophages and FBGCs decreased over the implantation period (Table 2). The SEM qualitative analysis illustrated a sequence of monocyte/macrophage and FBGC formation (Fig. 4) with an increase in the size of the FBGCs over time (Fig. 4B and C). The gold film showed greater macrophage adhesion than the other materials at day 4, while SU-8TM showed the lowest at the same time point (Table 2, Fig. 5). The acute inflammatory responses at day 7 were characterized by reduced number of cells (Table 2). Active macrophage fusion events were observed, as illustrated by initial cell aggregates due to macrophage migration (Fig. 6A), followed by an active fusion process where more macrophages were in the process of fusing with the initially generated FBGC (Fig. 6B). The number of macrophages and FBGCs declined at days 14 and 21 for all materials (Table 2). Morphologically, no differences in adherent macrophages or FBGCs adhesion on all surfaces at each time point were observed.

Based on leukocyte exudate analysis and cellular adhesion, the silicon wafer appears to be the least

biocompatible. The other materials, silicon dioxide, silicon nitride, gold, and SU-8TM are comparable in the induced inflammatory response, ranking their biocompatibility higher than that of the silicon wafer.

The SEM analysis of the material surfaces revealed a process of mechanical delamination specific to the SU-8TM material at late time points (Fig. 7). No mechanical delamination was observed with the other materials.

FBGCs were found to completely cover some of the MEMS wells, as illustrated by Fig. 8. The SEM analysis

could not determine whether the FBGCs developed over an intact or ruptured gold membrane.

4. Discussion

The MEMS component materials were found to be biocompatible and exhibited reduced biofouling based on exudate and surface analyses. Overall, the inflammatory responses elicited by these materials were not statistically significantly different than those for the empty cage controls over the duration of the study. Also, the sequence of monocyte/macrophage and FBGC formation (Fig. 6) was similar to those previously observed with National Heart, Lung, and Blood Institute reference materials polyethylene [15] and polydimethylsiloxane [16] and numerous biocompatible polyurethane materials [17] considered as candidates for biomedical applications.

The macrophage concentration in the exudate at day 21 of the silicon surface explains the increased surface density of those cells compared to the other materials at the same time point. Nevertheless, the macrophage concentration in the exudate at day 21 is lower than that of medical grade polyethylene at the same time point [15].

The silicon nitride and silicon dioxide were comparable in their inflammatory response and biofouling behavior. Therefore, the choice of dielectric between silicon nitride and silicon dioxide will depend on mechanical and fabrication properties.

Table 2
In vivo macrophage and FBGC surface densities on MEMS candidate materials. (Cell density^a: cells per mm²)

Material	Cell Type	Day 4	Day 7	Day 14	Day 21
Gold	Macrophages	168 ± 17	42 ± 8	3 ± 1	3 ± 1
	FBGCs	0	35 ± 12	14 ± 5	5 ± 1
SiO ₂	Macrophages	98 ± 12	70 ± 14	4 ± 2	2 ± 1
	FBGCs	0	21 ± 4	14 ± 3	3 ± 1
Si ₃ N ₄	Macrophages	123 ± 17	37 ± 6	4 ± 0	6 ± 0
	FBGCs	0	8 ± 3	12 ± 3	3 ± 1
Si Wafer	Macrophages	96 ± 19	68 ± 12	25 ± 6	21 ± 3
	FBGCs	0	5 ± 1	7 ± 1	3 ± 1
SU-8	Macrophages	72 ± 19	56 ± 17	2 ± 0	3 ± 1
	FBGCs	0	15 ± 4	7 ± 1	12 ± 2

^a Five 1 × 1 mm grids per sample for 3 samples, *n* = 15.

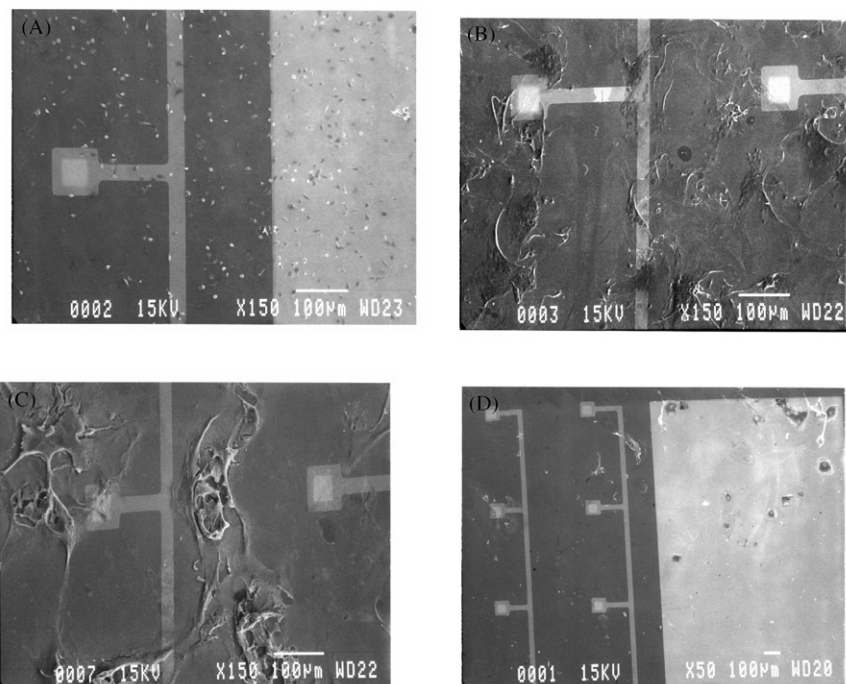


Fig. 4. Silicon dioxide SEM photomicrographs at explant days 4, 7, and 14. The macrophages at day 4 (A—150 ×) undergo a process of migration and fusion at day 7 and 14 generating larger FBGCs, over time (B, C—150 ×).

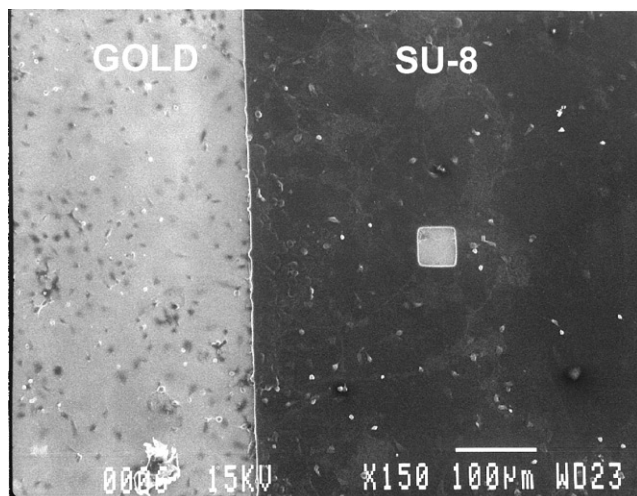


Fig. 5. SU-8/gold SEM photomicrograph showing preferential adhesion of macrophages onto the gold cathode compared to the SU-8™ insulating film (150 \times , day 4).

While the SU-8™ appeared to be a biocompatible material, it did undergo delamination at later time points. It appears that the delamination was initiated at the corners of the material resulting in its acquired folding. Even though SU-8™ may be biocompatible, the *in vivo* delamination process excludes it as a potential silicon wafer photoresist due to its reduced bonding capacity. However, the investigation of alternative bonding methods that may alleviate such problems are in progress.

One of the desired characteristics in an MEMS drug delivery device is the ability to generate a complex and fully controlled release profile of multiple therapeutic agents. It has been suggested that increased cellular adhesion, observed here by large numbers of surface macrophages and FBGCs, may impede the long-term functionality of such a device [10,14]. The results of this study suggest using silicon dioxide or nitride as dielectrics to minimize possible interference on the working device due to increased cellular adhesion (Table 2). Additionally, it would be advantageous for the silicon to undergo a surface modification process such as passivation or silanation [18]. Desai et al. reported the biocompatibility of microfabricated immunisolating silicon capsules *in vitro* for up to 1 month [19]. Based on insulin release studies of encapsulated islets, it was concluded that the devices were biocompatible. The *in vivo* studies confirm the *in vitro* findings, however, caution on the level of silicon wafer biocompatibility and suggest surface treatments to enhance its *in vivo* performance. Weisenberg and Mooradian reported the reduced hemocompatibility of silicon, silicon nitride, and SU-8™, as well as the increased hemocompatibility of silicon dioxide compared to polyurethane controls, *in vitro* [20]. It is difficult to interpret our results vis-à-vis

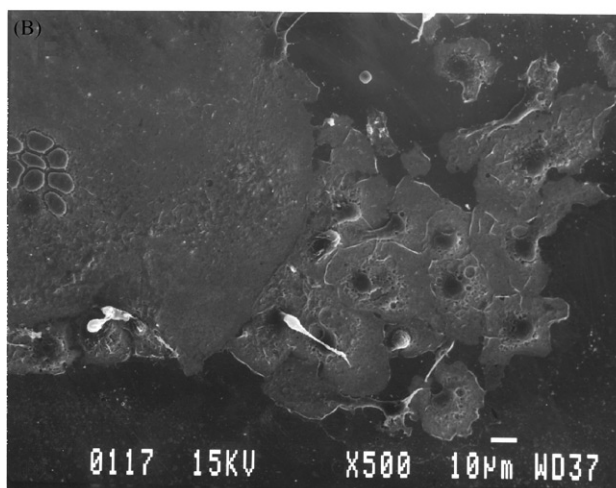
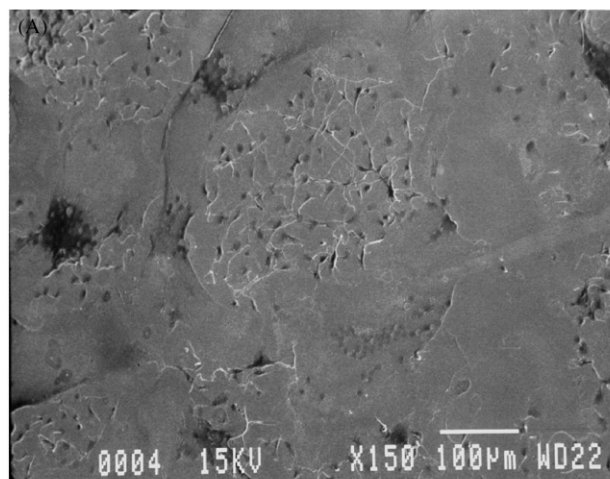


Fig. 6. SEM photomicrographs illustrate fusion of macrophages into (FBGCs). The macrophages initially aggregate (A—150 \times , day 7, silicon dioxide), where the individual cells have not yet fused their cytoplasm. Following cytoplasmic fusion, the individual nuclei migrate typically toward the center of the newly formed FBGC (B—50 \times , day 14, silicon dioxide). Then, the FBGC increases in size due to fusion of the newly migrated macrophages to the existing giant cell (B—50 \times , day 14, silicon dioxide).

the *in vitro* findings because our devices were not assessed in terms of hemocompatibility. However, it is interesting to summarize the *in vitro* findings as an emphasis to the importance of considering clinical application a vital parameter in the design of MEMS.

Others have reported on the potential corrosion *in vivo* of a silicon oxide passivating layer occurring as early as 1 month in a sensor array, reducing the overall biocompatibility of the device over time [18,21,22]. Kristensen et al. have recently reported on the biocompatibility and biofouling of an implantable silicon-based stimulator to treat paralysis of the larynx for periods ranging from 6 to 12 months [22]. Based solely on histological analysis, it was concluded that the devices

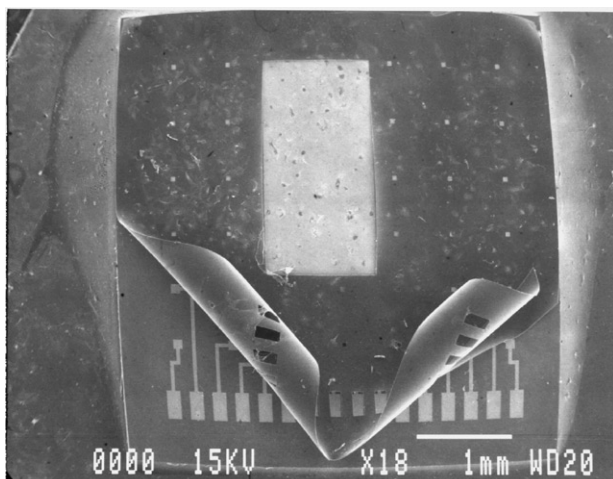


Fig. 7. SEM photomicrograph illustrating the mechanical delamination of SU-8™ at 21 days (18 \times).

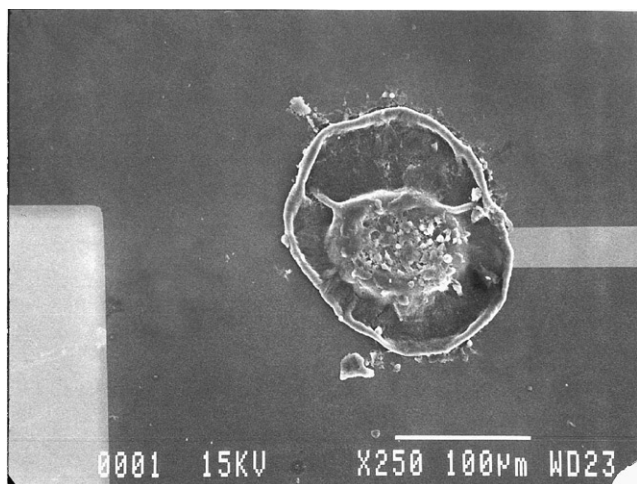


Fig. 8. SEM photomicrographs illustrating a FBGC atop a delivery microwell. It is not evident if the gold membrane sealing the microwell is still present (250 \times , silicon dioxide, day 4).

were well tolerated and resulted in a minimal foreign body response in the host. The studies described above relied only on qualitative histological and/or surface analyses to investigate biocompatibility and biofouling.

The *in vivo* analyses presented in this paper consisting of exudate and cell surface quantification constitute a more complete approach to assessing biocompatibility and biofouling of a device, and provide the expanding field of microprocessed implant devices with an important material selection tool. The unique characteristics of the cage system provide a standard inflammatory environment in which the biocompatibility of a material can be studied temporally in terms of humoral and cellular responses, cell–material interactions, FBGC formation kinetics, and biostability of materials without the mechanical interference of the surrounding tissue.

5. Conclusions

The present study has identified the MEMS drug delivery device component materials, gold, silicon nitride, silicon dioxide, SU-8™, and silicon as biocompatible, with gold, silicon nitride, silicon dioxide, and SU-8™ showing reduced biofouling.

Acknowledgements

This study was kindly supported by US National Institutes of Health Grant No. 1 R24 AI47739-01. R.S.S. was supported by a National Science Foundation Fellowship. All microfabrication work was carried out at the Microsystems Technology Laboratory at MIT. The technical assistance of Elizabeth Christenson is gratefully acknowledged.

References

- [1] Kimura J, Kuriyama T. FET biosensors. *J Biotech* 1990;15(3): 239–54.
- [2] Hernández PR, Taboada C, Leija L, Tsutsumi V, Vázquez B, Valdés-Perezgasga F, Reyes JL. Evaluation of biocompatibility of pH-ISFET materials during long-term subcutaneous implantation. *Sens Act B* 1998;46:133–8.
- [3] Certa U, Hochstrasser R, Langen H, Buess M, Moroni C. Biosensors in biomedical research: development and applications of gene chips. *Chimia* 1999;53:57–61.
- [4] Snyder JD, Desai TA. Microscale three-dimensional polymeric platforms for *in vitro* cell culture systems. *J Biomater Sci Polym E* 2001;12(8):921–32.
- [5] Turner JN, Shain W, Szarowski DH, Anderson M, Martins S, Isaacson M, Craighead H. Cerebral astrocyte response to micromachined silicon implants. *Exp Neurol* 1999;156:33–49.
- [6] Edell DJ, Toi VV, McNeil VM, Clark LD. Factors influencing the biocompatibility of insertable silicon microshafts in cerebral cortex. *IEEE Trans Biomed Eng* 1992;39(6):635–43.
- [7] Dario P, Carrozza MC, Benvenuto A, Menciassi A. Microsystems in biomedical applications. *J Micromech Microeng* 2000;10:235–44.
- [8] McAllister DV, Allen MG, Prausnitz MR. Microfabricated microneedles for gene and drug delivery. *Annu Rev Biomed Eng* 2000;2:289–313.
- [9] Leoni L, Desai TA. Nanoporous biocapsules for the encapsulation of insulinoma cells: biotransport and biocompatibility considerations. *IEEE Trans Biomed Eng* 2001;48(11):1335–41.
- [10] Santini Jr. JT, Cima MJ, Langer R. A controlled release microchip. *Nature* 1999;397(6717):335–8.
- [11] Anderson JM, Langone JJ. Issues and perspectives on the biocompatibility and immunotoxicity evaluation of implanted controlled release systems. *J Control Release* 1999;57(2):107–13.
- [12] Anderson JM. Inflammation, wound healing and the foreign body response. *Biomaterials science: an introduction to materials in medicine*. San-Diego, CA: Academic Press Inc., 1996 [chapter 4(4.2)].
- [13] Shaw JM, Gelorme JD, LaBianca NC, et al. Negative photoresists for optical lithography. *IBM J Res Develop* 1997;41(1/2):81–94.
- [14] Santini JT, Richards AC, Scheidt RA, Cima MJ, Langer R. Microchips as controlled drug delivery devices. *Ang Chem Int Ed* 2000;39:2396–407.

- [15] Spilizewski KL, Marchant RE, Anderson JM, Hiltner A. In vivo leukocyte interactions with NHLBI-DTB primary reference materials: polyethylene and silica-free polydimethylsiloxane. *Biomaterials* 1987;8(1):12–7.
- [16] Belanger MC, Marois Y. Hemocompatibility, biocompatibility, inflammatory and in vivo studies of primary reference materials low-density polyethylene and polydimethylsiloxane: a review. *J Biomed Mater Res* 2001;58(5):467–77.
- [17] Brunstedt MR, Ziats NP, Schubert M, Stacks S, Rose-Caprara V, Hiltner PA, Anderson JM. Protein adsorption and endothelial cell attachment and proliferation on PAPI-based additive modified poly(ether urethane ureas). *J Biomed Mater Res* 1993;27(4):499–510.
- [18] Hämmerle H, Kobuch K, Kohler K, Nisch W, Helmut Sachs, Steltze M. Biostability of micro-photodiode arrays for subretinal implantation. *Biomaterials* 2002;23:797–804.
- [19] Desai TA, Chu WH, Tu JK, et al. Microfabricated immunisolating biocapsules. *Biotechnol Bioeng* 1998;57(1):118–20.
- [20] Weisenberg BA, Mooradian DL. Hemocompatibility of materials used in microelectromechanical systems: platelet adhesion and morphology in vitro. *J Biomed Mater Res* 2002;60(2):282–91.
- [21] Zealear DL, Garren KC, Rodriguez GR, Reyes JH, Huang S, Dokmeci MR, Najafi K. The biocompatibility, integrity, and positional stability of an injectable microstimulator for reanimation of the paralyzed larynx. *IEEE Trans Biomed Eng* 2001;48:890–7.
- [22] Kristensen BW, Noraberg J, Thiebaud P, Koudelka –Hep M, Zimmer J. Biocompatibility of silicon-based arrays of electrodes coupled to organotypic hippocampal brain slice cultures. *Brain Res* 2001;896:1–17.